Structurally encoded intraclass differences in EphA clustering drive distinct cell responses

Supplementary material

Elena Seiradake[1], Andreas Schaupp[2], Daniel del Toro Ruiz[2], Rainer Kaufmann[1, 3], Nikolaos Mitakidis[1], Karl Harlos[1], A Radu Aricescu[1], Rüdiger Klein[2] & E Yvonne Jones[1]

[1] Division of Structural Biology, Wellcome Trust Centre for Human Genetics, University of Oxford, Oxford, UK.

[2] Max Planck Institute of Neurobiology, Martinsried, Germany.

[3] Department of Biochemistry, University of Oxford, Oxford, UK

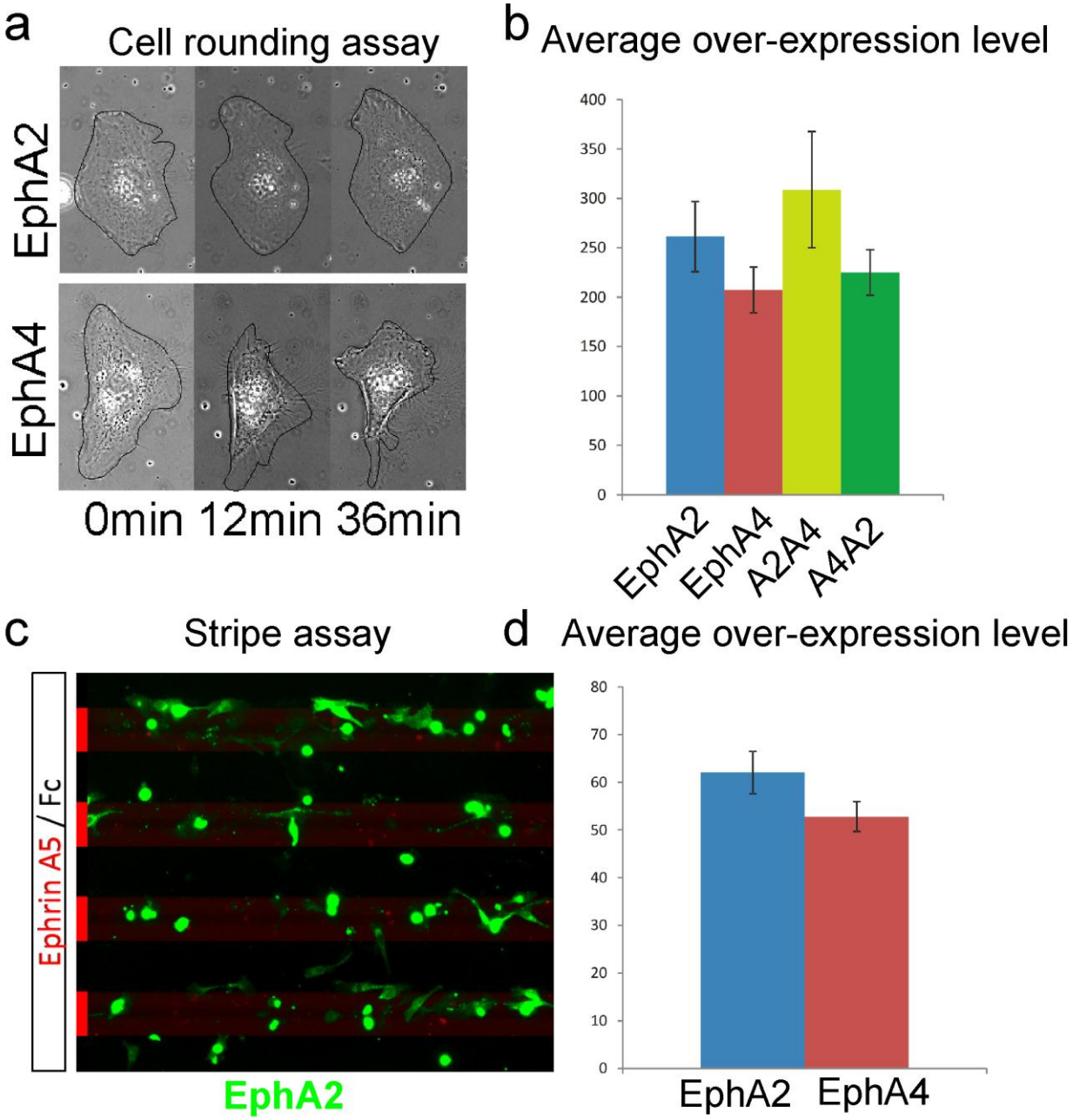
a
Cell rounding assay
EphA2
EphA4
0min 12min 36min
b Average over-expression level
400
350
300
250
200
150
100
50
0
EphA2
EphA4
A2A4
A4A2
c
Stripe assay
Ephrin A5 / Fc
EphA2
d Average over-expression level
80
70
60
50
40
30
20
10
0
EphA2 EphA4
e
Endogenous EphA2 and EphA4 expression
Western blot
RT-PCR
kDa
COS HeLa HEK-293
150
100
75
50
37
EphA4
actin
EphA2
PINK1

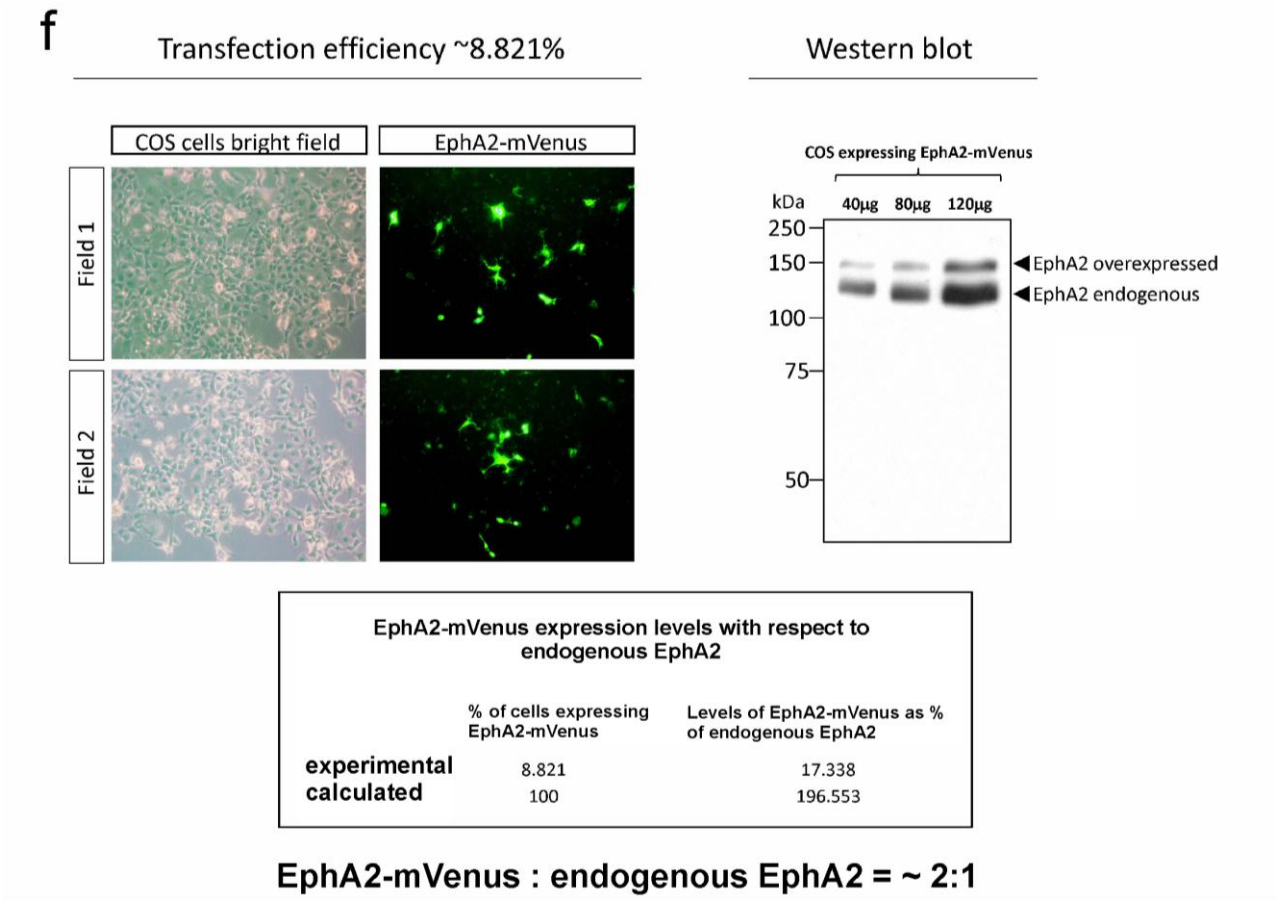

Supplementary Fig. 1. Evaluation strategy for the HeLa cell rounding assay. At least 40 cells were measured for the control and each construct before and at different time points after stimulation with ephrinA5-Fc. **a)** Adherent cell surfaces were measured using tools in the MetaMorph software package (Molecular Devices) using phase-contrast images. A black line encircles surfaces measured in the examples shown. **b)** To assess the average expression levels of mVenus-tagged EphA2- and EphA4- expressing cells, we used the corresponding fluorescent images, taken from the same cells before stimulation. The average fluorescent signal within encircled regions was measured for each cell ("average grey level") using MetaMorph. Using these data, we then calculated averages for all cells in each dataset. The corresponding s.e.m. (shown as bars) reflect the variability in expression levels within each dataset. **c)** mVenus-tagged EphA2-, EphA4- or control YFP-transfected cells were grown on alternating stripes of ephrinA5-Fc (red stripes) and Fc (black stripes). The images of cells were separated into two parts (on red or black stripes). **d)** The total number of YFP+ pixels (deriving from mVenus or YFP expressing cells) on red stripes was quantified using ImageJ. Results are presented as percentage of YFP+ pixels on red stripes with respect to total YFP+ pixels (main text **Fig. 1c**). The mVenus (YFP+) fluorescent signal for the different images was averaged using ImageJ ("average grey level") and is shown in the panel on the right. The corresponding s.e.m., reflecting the variability in expression levels in each dataset, are plotted. **e)** We analysed endogenous levels of EphA2 and EphA4 in lysates of COS7, HeLa and HEK297 cells using western blots and RT-PCR. Western blot in total cell lysates were performed as indicated: anti-EphA4 (mouse 1/1000; Invitrogen) and anti-EphA2 (rabbit 1/500; Santa Cruz). RT-PCR was performed using the following primers: EphA2: forward=CATTAAGGACTCGGGGCAGG, reverse=GGTCCCACCCTTTGCCATAC; EphA4: forward=ACCCCGCGAATGAAGTTACC, reverse=TTGACACAGGAGCCTCGAAC and for PINK1: forward=TGGAATATCTCGGCAGGTTC, reverse=GATGATGTTAGGGTGTGGGG). The data show that our HeLa cells express neither EphA2 nor EphA4, while our COS7 cells express EphA2 only. Our HEK cells, which were used only for large scale protein production for crystallization, express EphA4. As controls, we analysed the actin expression or PTEN-induced putative kinase 1 (PINK1) mRNA levels. **f)** We compare the expression levels of transfected EphA2-mVenus with respect to endogenous EphA2 in COS7 cultures. The transfection efficiency was estimated by measuring the ratio of EphA2-mVenus transfected/untransfected cells (~8.8%). After that, the cells were processed by western blot using anti-EphA2 antibody. Taking into account the transfection efficiency, on average, in transfected cells, the expression level of endogenous EphA2 is about 50% compared to that of over-expressed mVenus-tagged EphA2.

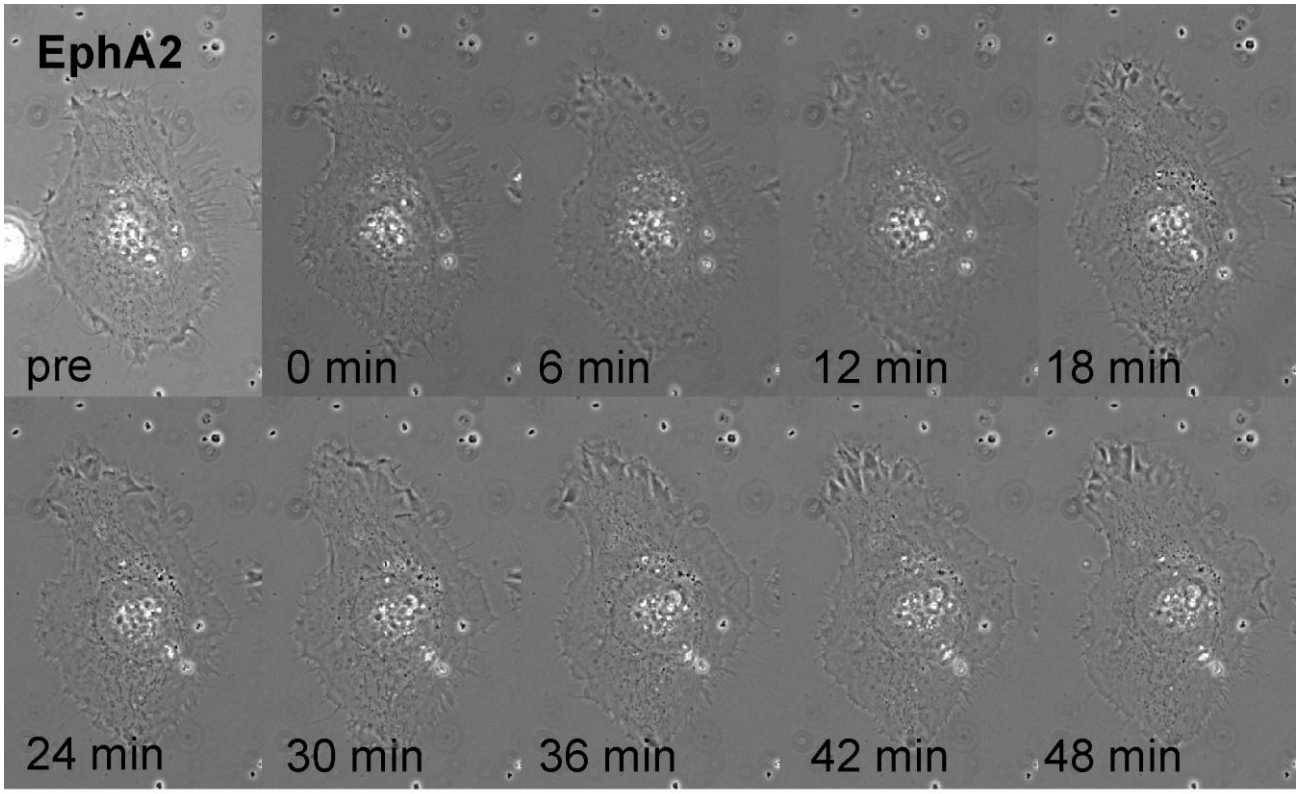
EphA2
pre
0 min
6 min
12 min
18 min
24 min
30 min
36 min
42 min
48 min

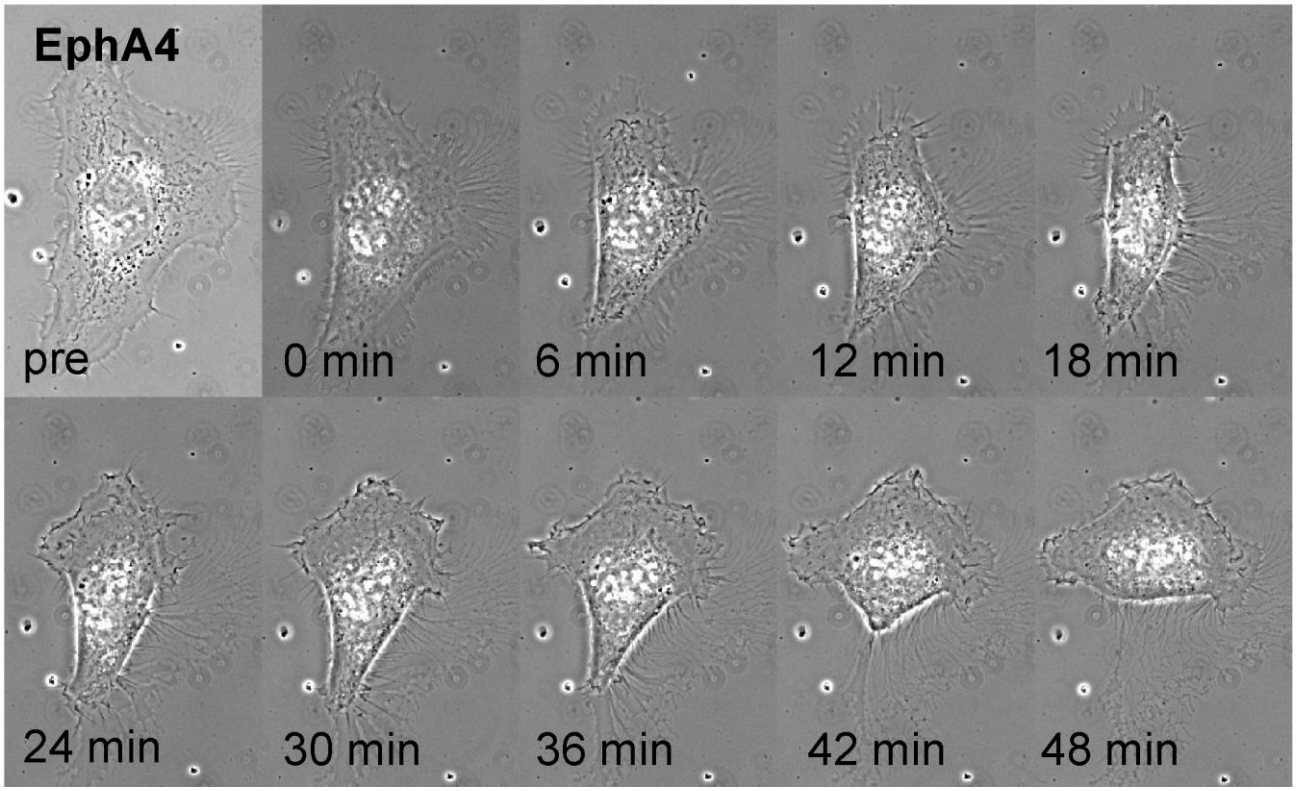
EphA4
pre
0 min
6 min
12 min
18 min
24 min
30 min
36 min
42 min
48 min

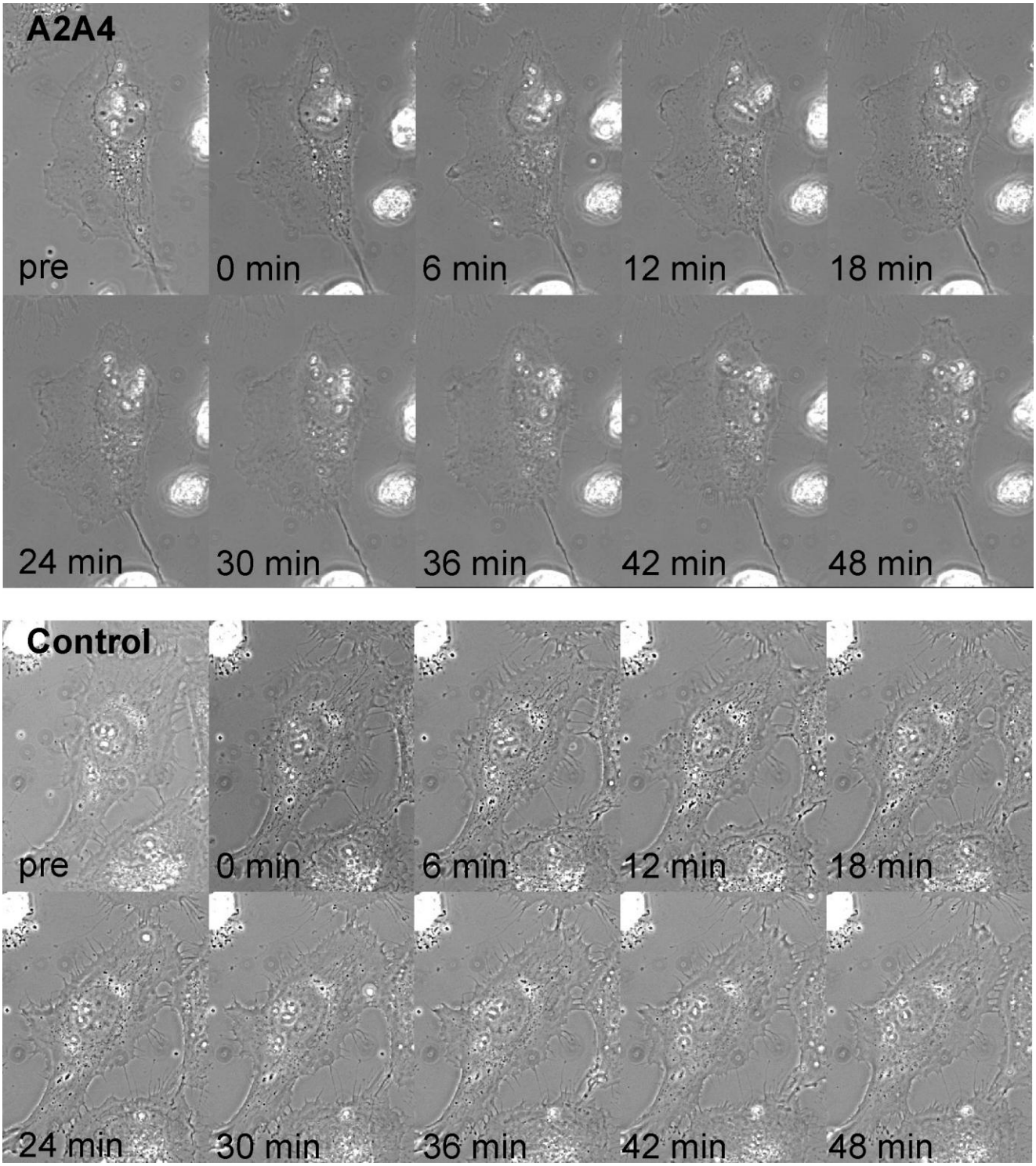

Supplementary Fig. 2. HeLa cell rounding assay. Transfected (or non-transfected control) HeLa cells were imaged before (pre) and every 6 minutes after stimulation with pre-clustered ephrinA5-Fc. Constructs containing the EphA2 ectodomain induced less cell rounding in response to stimulation compared to constructs containing EphA4 ectodomain. Example phase-contrast images are shown for EphA2-, EphA4-, A2A4-transfected cells and the control. In **Supplementary movies 1** and **2** images for EphA2- and EphA4-transfected cells are assembled into time lapse movies, respectively.

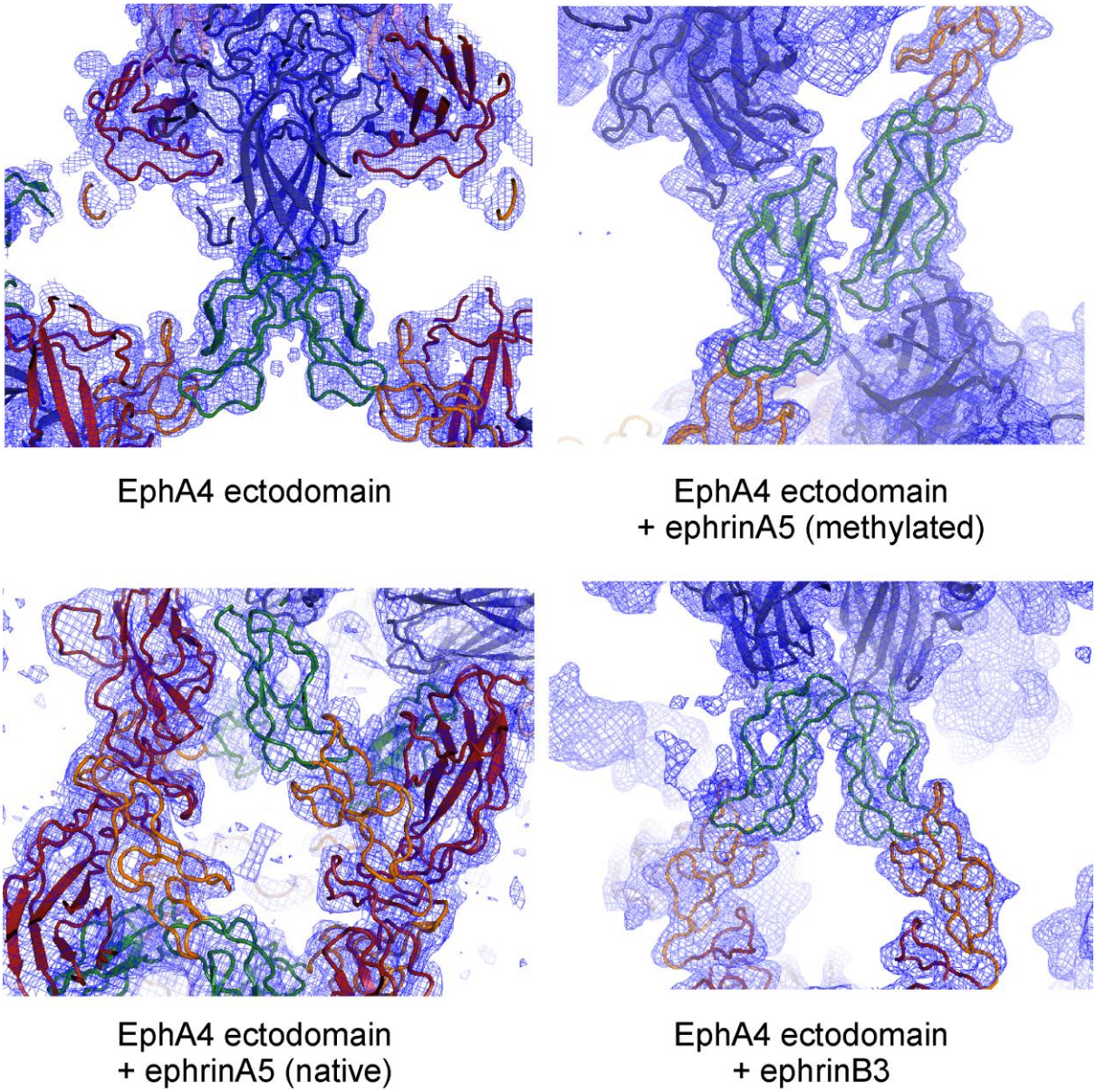

Supplementary Fig. 3. Electron density maps (2Fo-Fc) are represented as a blue mesh at the 1 σ level using solvent flattening of refinement solutions. Protein models are shown as cartoons, and coloured by domain (LBD =dark blue, sushi = green, EGF =orange/yellow, FN1 =dark red, FN2 =pink).

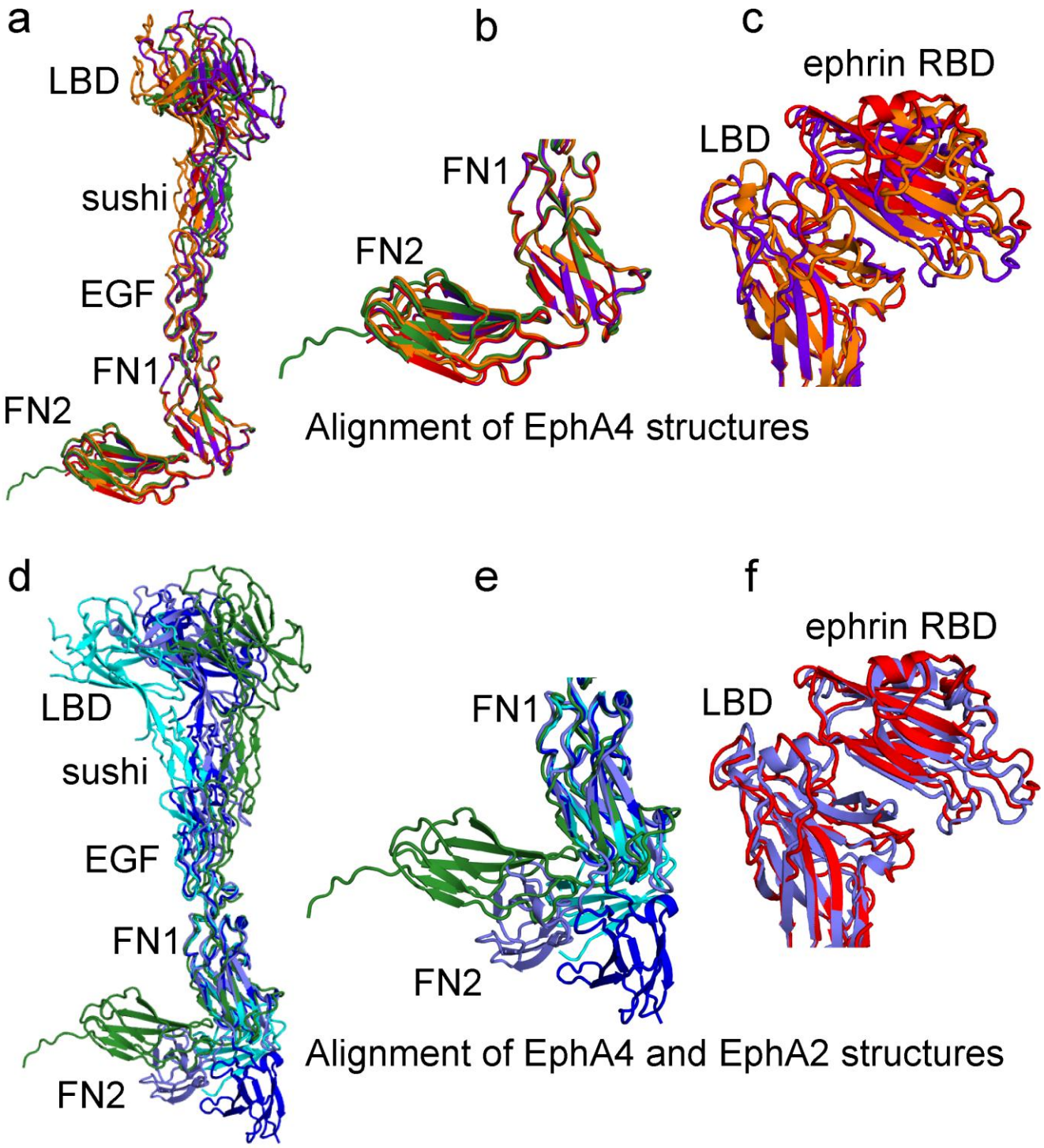

Supplementary Fig. 4. Schematic representation of superimposed EphA4 and EphA2 ectodomain models. The models are shown as cartoons and in different colours: unliganded native EphA4 (green), native EphA4 + ephrinB3 (orange), methylated EphA4 + ephrinA5 (red), native EphA4 + ephrinA5 (purple), unliganded methylated EphA2 (blue)[4], unliganded native EphA2 (cyan)[5], methylated EphA2 + ephrinA5 (slate)[4]. **a)** The four ectodomain structures of EphA4 were aligned using the FN1 domain. Ephrins are not shown. **b)** As panel a, but zoomed onto the FN1–FN2 domains. **c)** The structures of EphA4 ectodomain in complex with RBDs of ephrinA5 or ephrinB3 were aligned using the EphA4 LBD domain. Due to the plastic nature of the EphA4 LBD, ephrins can adopt slightly shifted conformations in the different structures. **d)** The ectodomain of unliganded EphA4 (green) and the three known ectodomain structures of EphA2 were aligned via the FN1 domain. Due to the flexibility in the EphA2 FN1–FN2 linker region, the FN2 domain differs in the three EphA2 structures. Ephrins are not shown. **e)** As panel d, but zoomed onto the FN1–FN2 domains. **f)** The structure of methylated EphA4 and EphA2 ectodomain (red and slate, respectively) in complex with ephrinA5 RBD were aligned using the LBD domain.

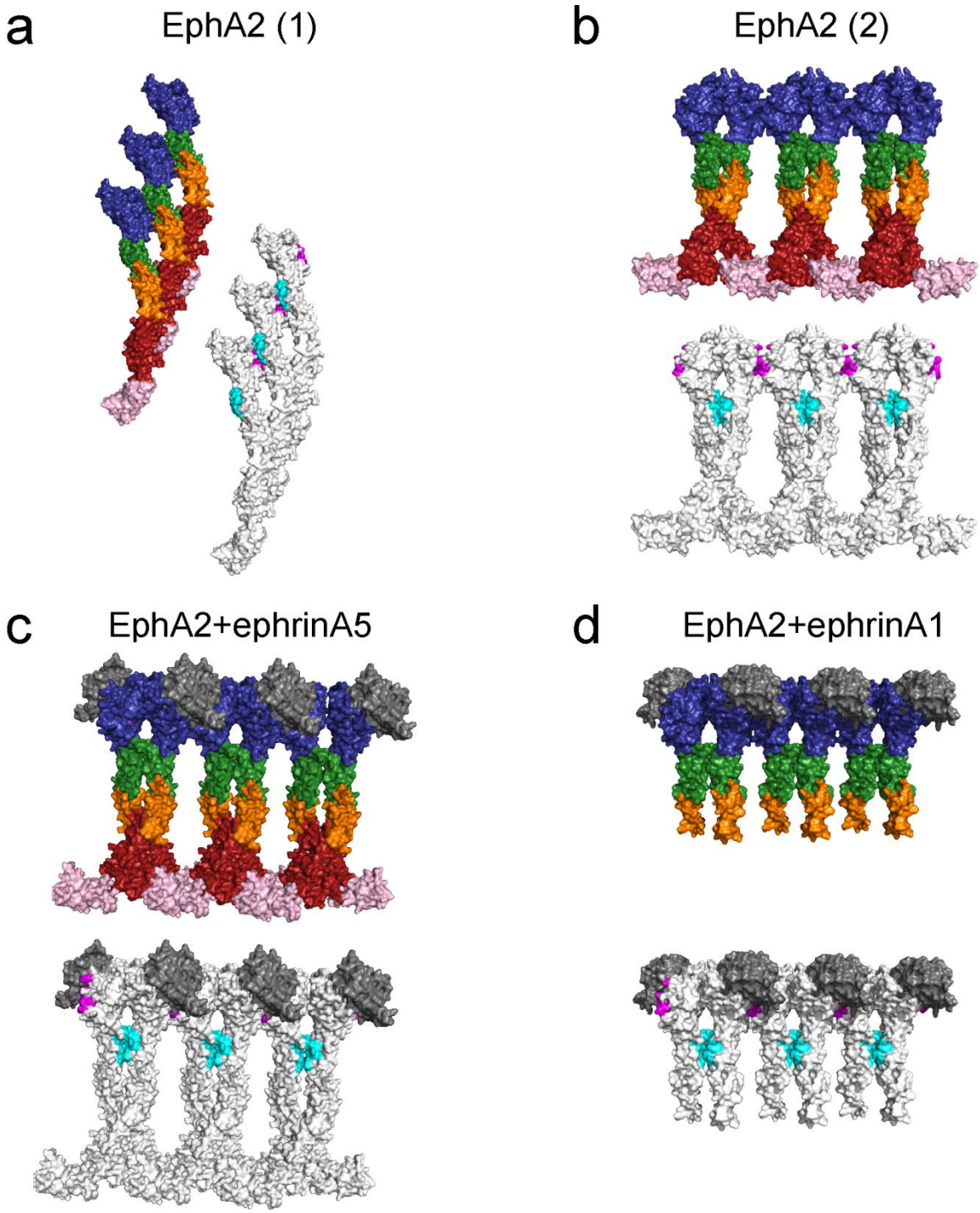

Supplementary Fig. 5. Unliganded and ephrin-bound $EphA2_{ecto}$ structures reveal array-like arrangements in the crystal lattice, mediated by EphA2–EphA2 contacts through regions on the sushi domain and the LBD[4,5]. EphA2 surface representations are coloured by domain (LBD =blue, sushi =green, EGF-like =orange, FN1 =red, FN2 =pink) or in white with contacting regions on the sushi domain and the LBD highlighted in cyan and magenta, respectively. EphrinA5 or A1 RBD are coloured in grey. **a)** Unliganded $EphA2_{ecto}$ (PDB accession code 2X10)[4]. **b)** Unliganded $EphA2_{ecto}$ (PDB accession code 3FL7)[5]. **c)** $EphA2_{ecto}$ in complex with ephrinA5 RBD (PDB accession code 2X11)[4]. **d)** EphA2 fragment comprising the LBD, sushi and EGF-like domains in complex with ephrinA1 RBD (PDB accession code 3MBW)[5].

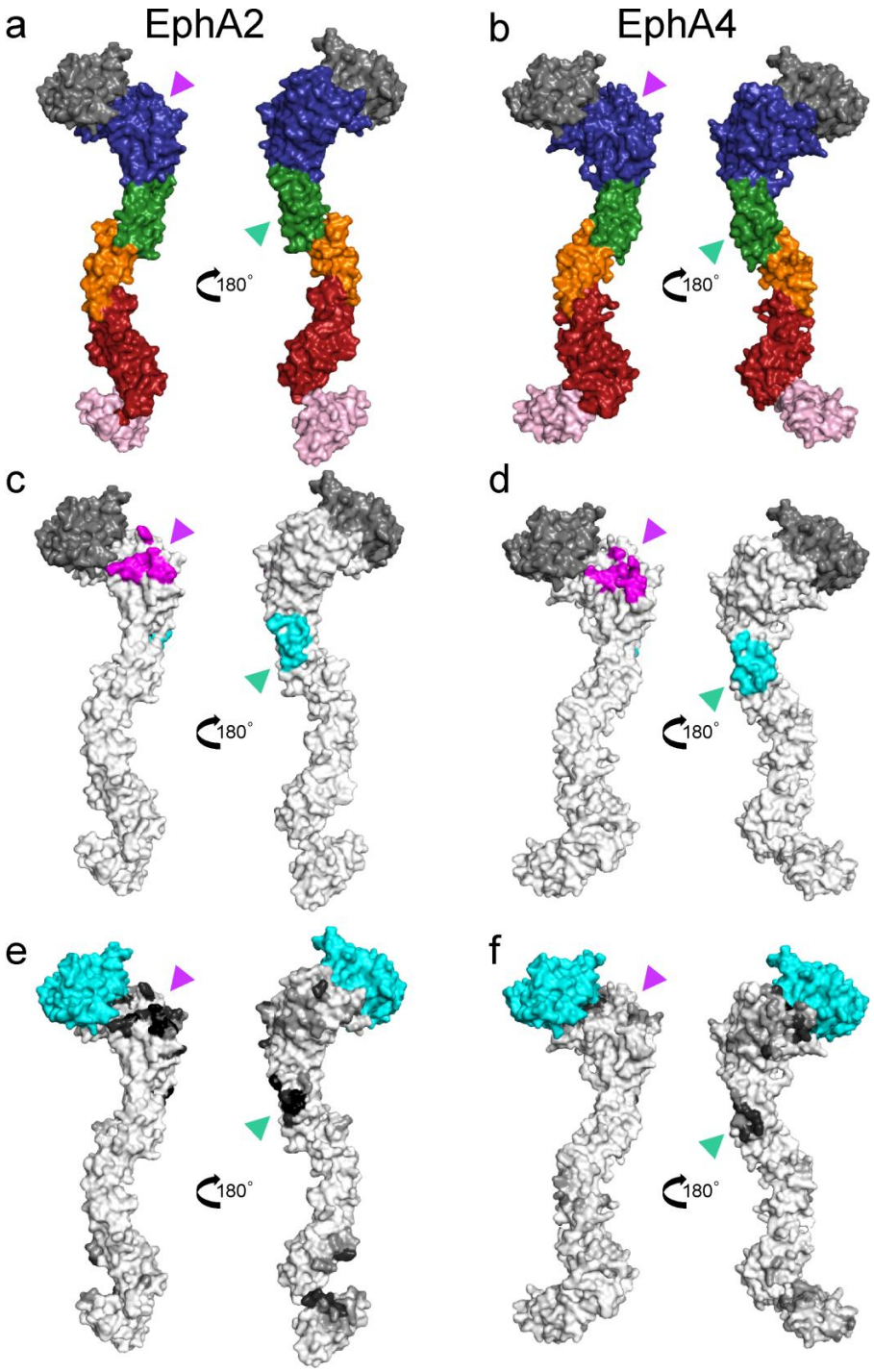

Supplementary Fig. 6. Surface representations of $EphA2_{ecto}$ and $EphA4_{ecto}$ in complex with ephrinA5 RBD are shown. Pink and blue arrows point to surfaces providing contacts in the $EphA2_{ecto}$ arrays on the LBD and the sushi domain, respectively. **a)** $EphA2_{ecto}$ in complex with ephrinA5 RBD. Colours are according to domain: LBD (dark blue), sushi (green), EGF-like (orange), FN1 (dark red), FN2 (light pink), ephrinA5 RBD (grey). **b)** As panel a, but showing the corresponding $EphA4_{ecto}$ structure. **c)** As panel a, but colours are white (EphA2), grey (ephrinA5), magenta (HI-loop and adjacent regions), cyan (sushi dimerisation surface). **d)** As panel c, but showing the corresponding $EphA4_{ecto}$ structure. **e)** As panel a, but the $EphA2_{ecto}$ surface is coloured according to the frequency of residues mediating lattice contacts in the four crystal structures known. Colours range from black = involved in all lattices, to white = not involved in any lattices. f) As panel e, showing frequencies for the corresponding $EphA4_{ecto}$ structures. Notably, residues in the EphA4 HI-loop are less frequently involved in mediating lattice contacts compared to those in the EphA2 HI-loop.

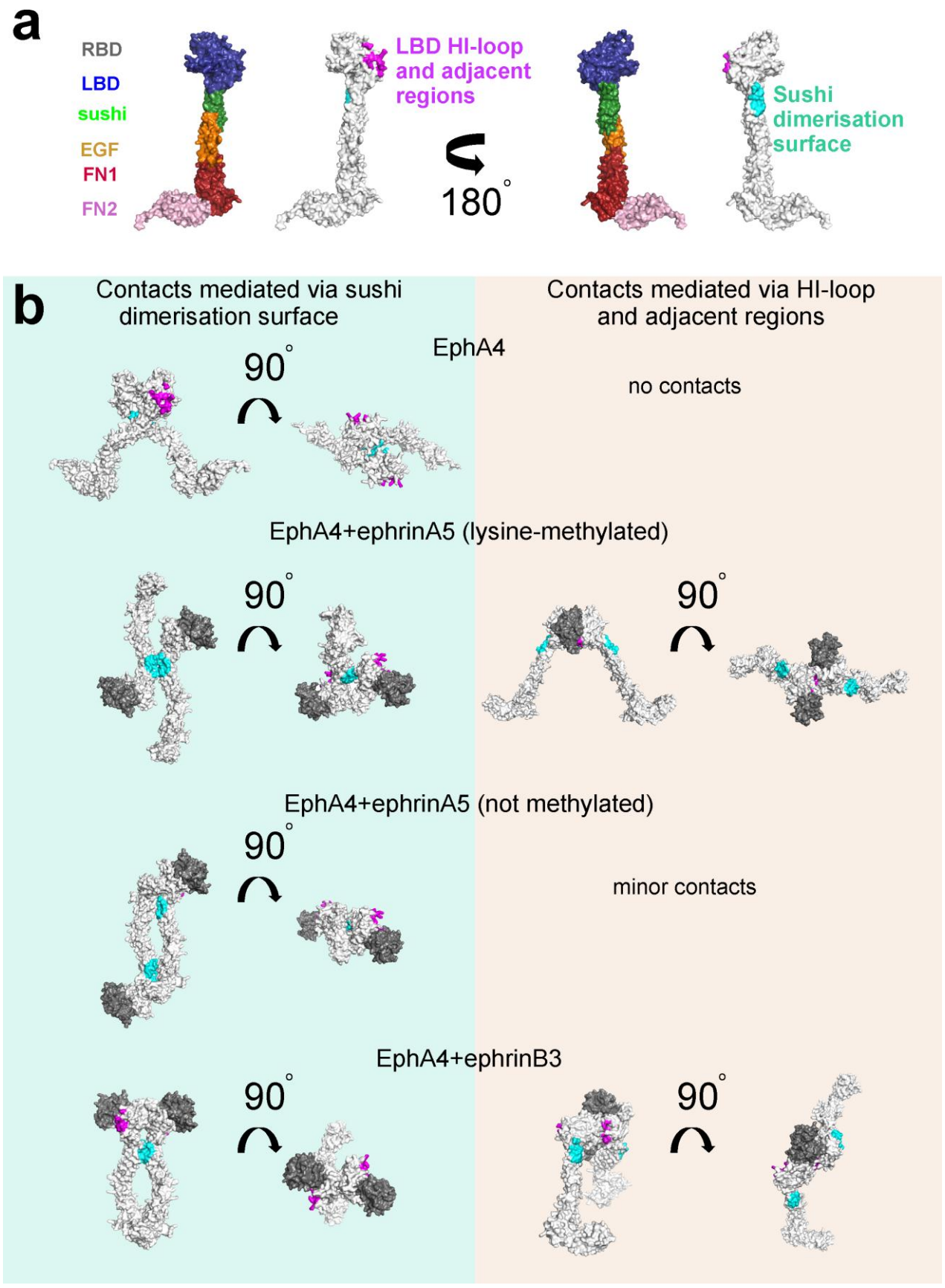

Supplementary Fig. 7. $EphA4_{ecto}$ crystal lattice contacts provided via the sushi dimerization surface and the LBD HI-loop area. **a)** The structure of unliganded $EphA4_{ecto}$ is coloured by domain, or in white with specific regions on the LBD and sushi domain highlighted in magenta and cyan, respectively. **b)** Copies of $EphA4_{ecto}$ (unliganded or in complex with ephrins) in contact via the two specified regions in the different lattices. $EphA4_{ecto}$ is coloured white with the two regions coloured in magenta and cyan. EphrinA5 RBD and ephrinB3 RBD are coloured grey.

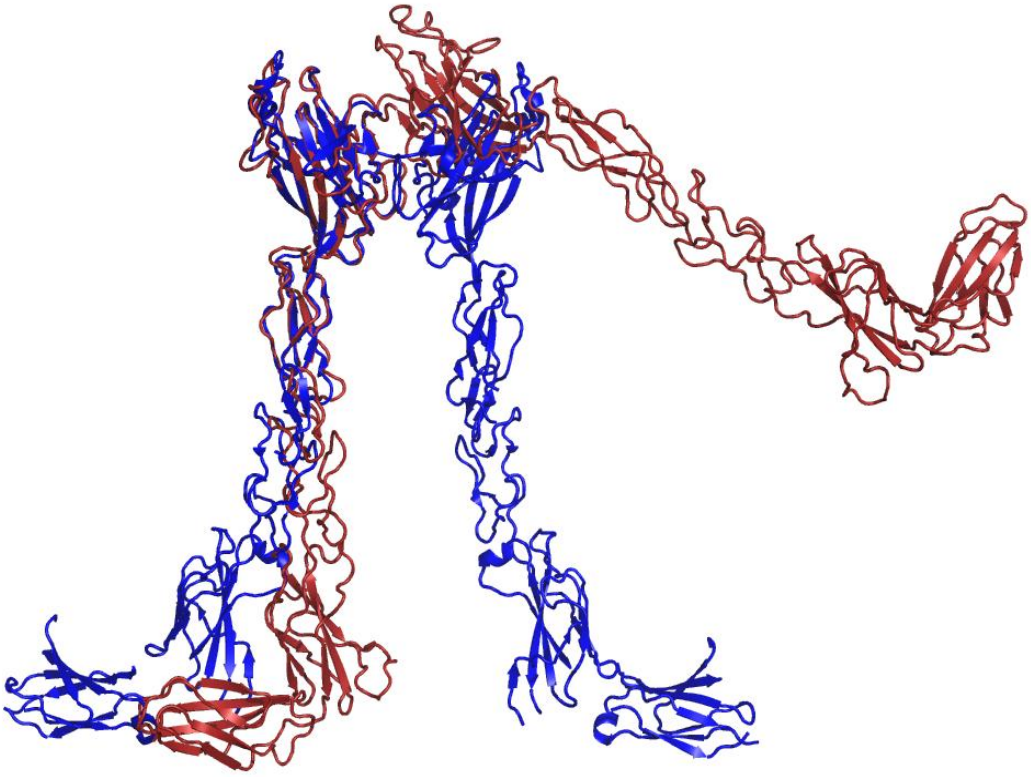

Supplementary Fig. 8. Dimeric arrangements mediated by the LBD in crystals of lysine-methylated ectodomains of EphA2 (blue)[4] and EphA4 (red) in complex with ephrinA5 RBD (not shown). The structures were superposed via the LBD domain of one of the two chains.

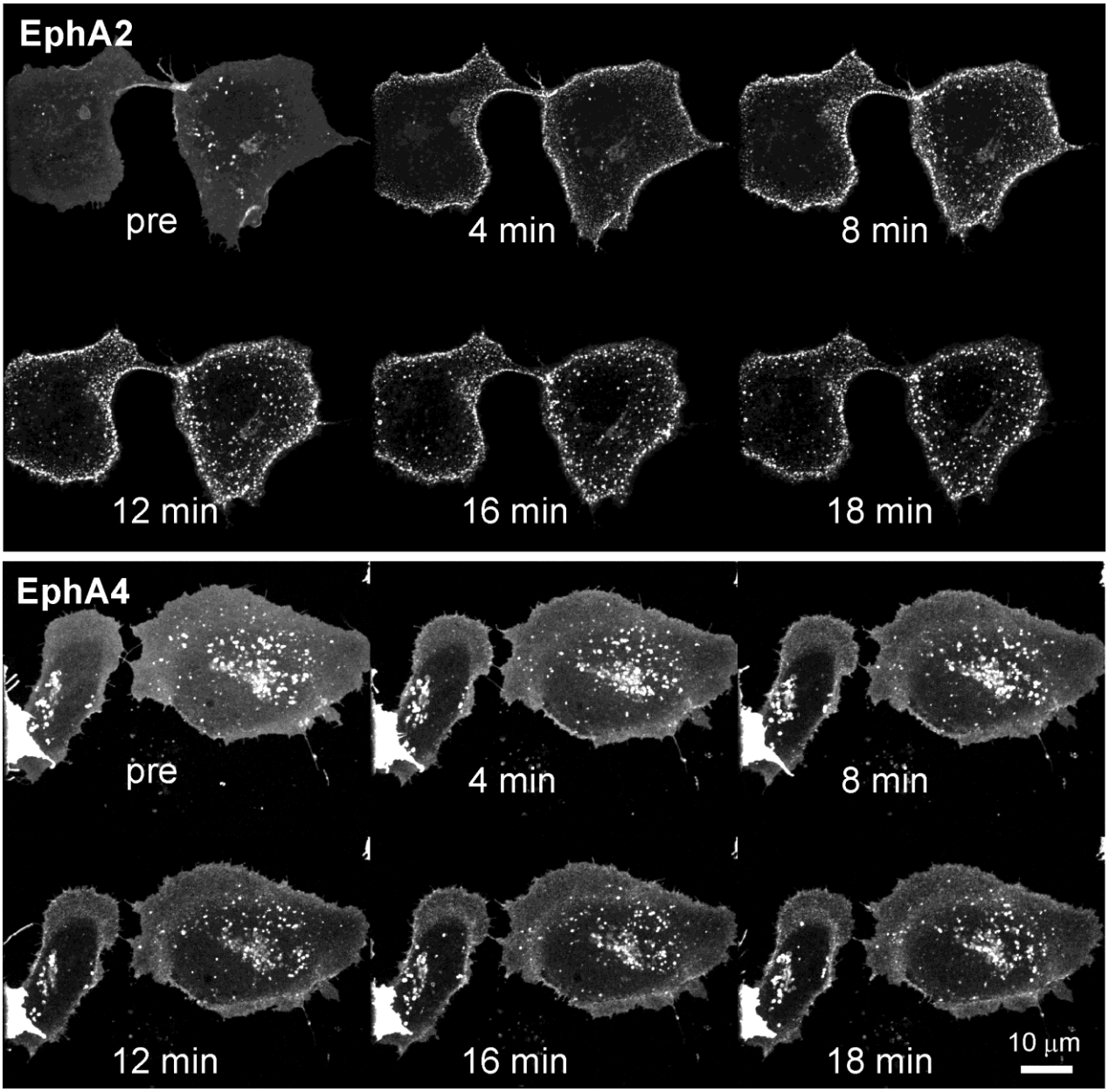
EphA2
pre
4 min
8 min
12 min
16 min
18 min

EphA4
pre
4 min
8 min
12 min
16 min
18 min
10 μm

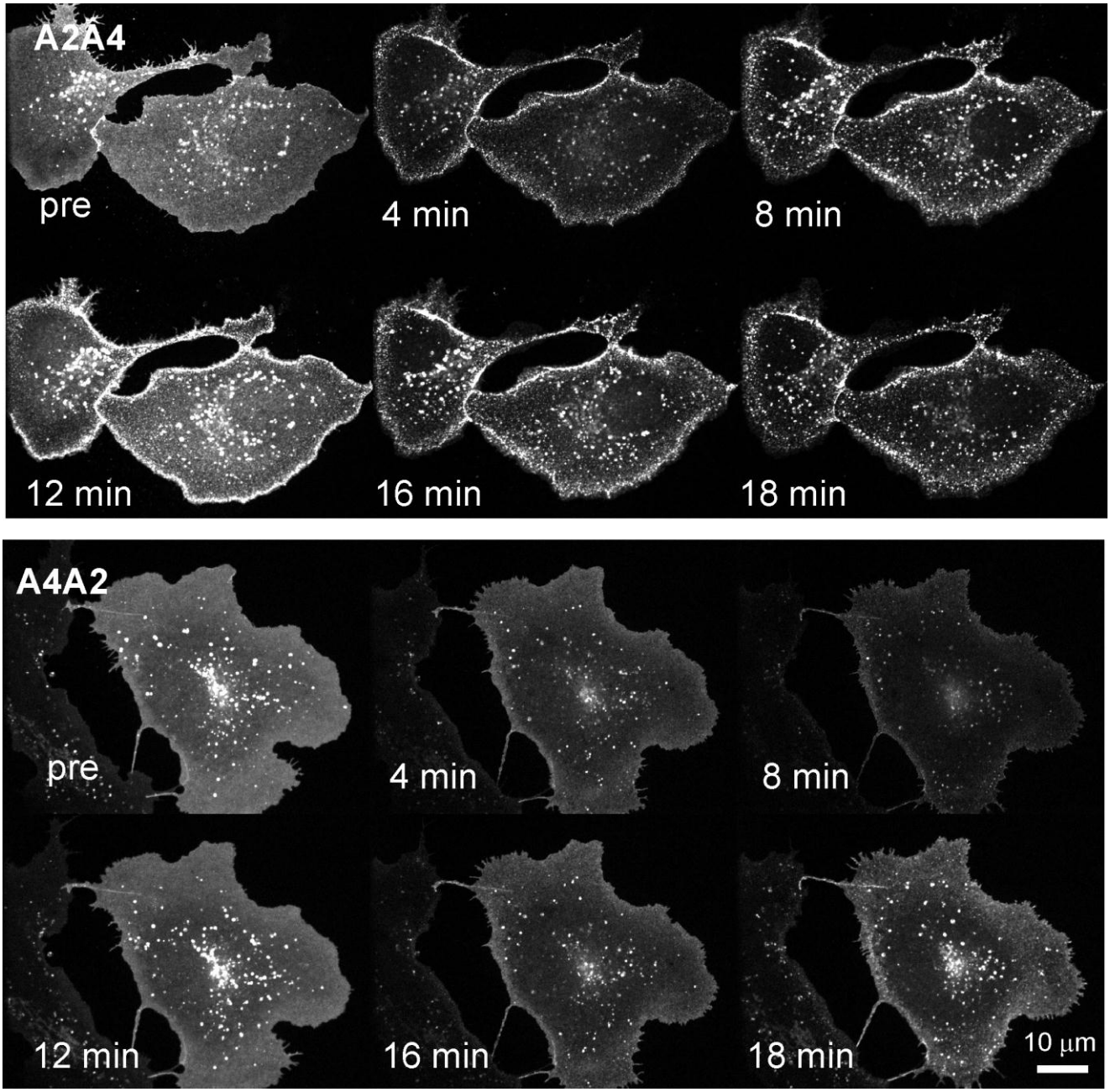

Supplementary Fig. 9. Eph clustering assay. Transfected COS 7 cells were imaged before (pre) and every 6 minutes after stimulation with pre-clustered ephrinA5-Fc using a spinning disc confocal microscope. Constructs containing the EphA2 ectodomain clustered more in response to stimulation compared to constructs containing EphA4 ectodomain. Before stimulation, Eph is homogenously distributed at the cell surface and is also present in large intracellular vesicles. The latter is due to overexpression and does not interfere with ephrin stimulation and the clustering analysis, where regions without intracellular vesicles, close to the cell periphery, were selected. The images corresponding to the above samples and additional mutant constructs were assembled into time lapse movies (**Supplementary movies 3–8)**.

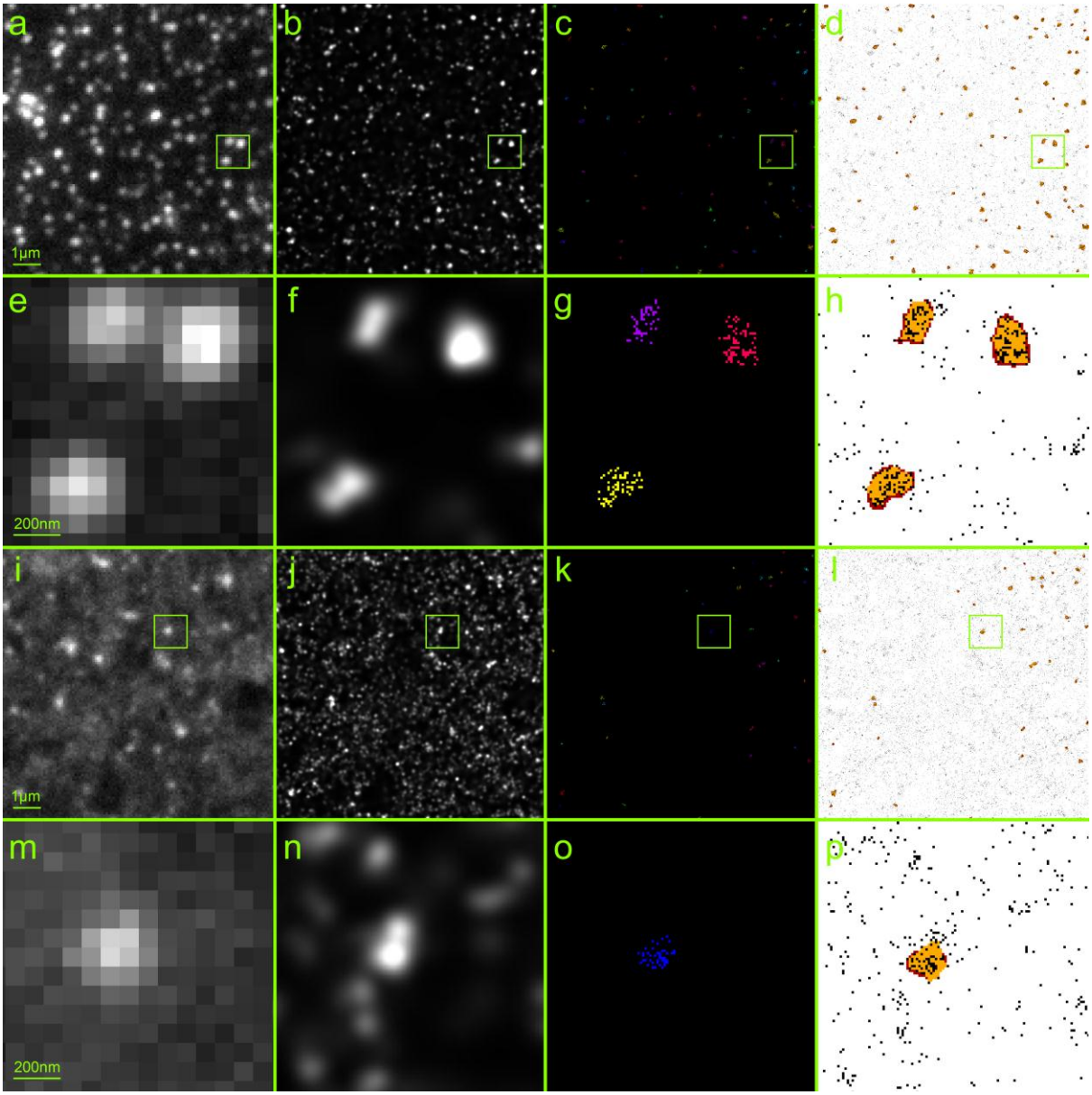

Supplementary Fig. 10. Localization microscopy data analysis. **a)** Conventional wide-field fluorescence image of mVenus-tagged chimeric construct A2A4 in COS7 cells. **b)** Localization microscopy image of the same area as in panel a. **c)** Scatter plot of single molecule positions having 20 or more neighbours within a radius of 50 nm. Those belonging to the same cluster are color coded accordingly. **d)** All detected single molecule positions are depicted by black dots. Clusters are marked in orange. **e) – h)** Magnified images of the regions marked in the images in the top panel. **i) – p)** Equivalent images for one measurement of construct A4A2.

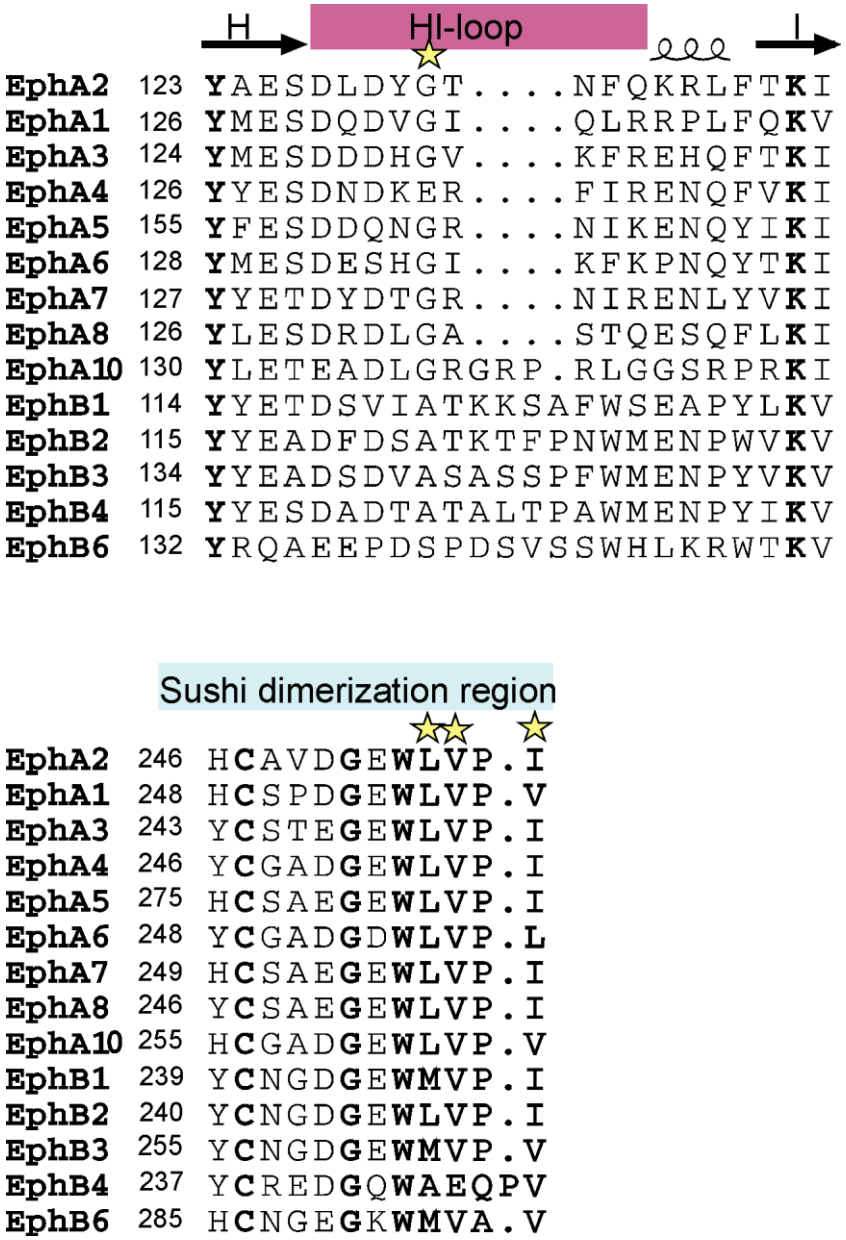

Supplementary Fig. 11. Sequence alignment of the HI-loop and a region in the sushi domain harbouring hydrophobic residues involved in Eph–Eph dimerization (human Eph sequences shown). The residues that are mutated in EphA2^{HI} (G131Y) and EphA2^{su} (L254D V255D I257D), located in HI-loop and the sushi dimerization surface, respectively, are marked with stars. The glycine at position 131 in EphA2 is conserved in all EphAs except EphA4. The hydrophobic residues and proline at positions 254–256 in the EphA2 sushi dimerization surface are generally conserved across EphAs and EphBs, with the exception of EphB4, suggesting that this Eph receptor may use this surface in a different way.

Supplementary Note

Preparation of complexes for crystallisation. Isolated human $EphA4_{ecto}$ and ephrin RBD proteins were purified from HEK293S GnTI$^-$ cell culture medium using Ni-affinity and size-exclusion chromatography as described in the **Online Methods**. We dialyzed cell medium against phosphate buffer saline and loaded it onto a Ni-containing affinity column (His-Trap, GE Healthcare). We then washed the column with 20mM Tris pH 7.5, 300mM NaCl, 40mM imidazole and eluted the protein with 20mM Tris pH 7.5, 300mM NaCl, 230mM imidazole.

To produce $EphA4_{ecto}$ + ephrinA5 complexes, we mixed the proteins in a 1:1.5 molar ratio and incubated the proteins at room temperature with 1:20 recombinant endoglycosidase F1[6,7] overnight. To remove the endoglycosidase, we diluted the protein 1:10 with 20mM Tris pH 7.5, 300mM NaCl, re-loaded it on a Ni-containing column, washed and re-eluted. We concentrated the eluted protein and loaded it on a Superdex 200 column (GE Healthcare) previously equilibrated with crystallization buffer 1 (150 mM NaCl, 20mM Tris pH 7.5) for generation of native $EphA4_{ecto}$ + ephrinA5 RBD crystals or pre-methylation buffer (250 mM NaCl, 50 mM Hepes pH 7.5) for subsequent lysine-methylation using previously established protocols[8]. We added 100mM Tris pH 7.5 after the end of the methylation reaction and purified the methylated sample on a Superdex 200 column previously equilibrated with crystallization buffer 2 (200 mM NaCl, 20mM Tris pH 7.5). We pooled fractions containing methylated or native $EphA4_{ecto}$ + ephrinA5 complexes and concentrated these to 9.8 and 9.3 mg ml^{-1}, respectively, for crystallization.

To generate native EphA4ecto + ephrinB3 RBD complexes, we incubated the proteins separately at room temperature with 1:20 recombinant endoglycosidase F1[6,7] overnight. To remove the endoglycosidase, we diluted the protein 1:10 with 20mM Tris pH 7.5, 300mM NaCl, re-loaded it on a Ni-containing column, washed and re-eluted. We concentrated the eluted proteins and loaded them separately on a Superdex 200 column (GE Healthcare) previously equilibrated with crystallization buffer 1 (150mM NaCl 20mM Tris 7.5). Before crystallization, EphA4ecto and ephrinB3 RBD were then mixed in a 1:1 molar ratio and concentrated to 8.8 mg ml^{-1}.

The crystals of native unliganded $EphA4_{ecto}$ grew in drops containing a 1:1 mixture of $EphA4_{ecto}$ and polyhistidine-tagged human ephrinB2 RBD. Indeed, we were unable to produce diffracting crystals of $EphA4_{ecto}$ in the absence of ephrinB2 RBD. The sample was generated using the same procedure as for $EphA4_{ecto}$ in complex with ephrinB3 RBD. Proteins were de-glycosylated and then purified separately on a Superdex 200 column previously equilibrated with crystallization buffer 1. $EphA4_{ecto}$ and ephrinB2 RBD were then mixed in a 1:1 molar ratio and concentrated to 5.8 mg ml^{-1} for crystallization.

Supplementary References:

1 Bowden, T. A. *et al.* Structural plasticity of eph receptor A4 facilitates cross-class ephrin signaling. *Structure* **17**, 1386–1397. (2009).

2 Noberini, R., Rubio de la Torre, E. & Pasquale, E. B. Profiling Eph receptor expression in cells and tissues: a targeted mass spectrometry approach. *Cell Adh Migr* **6** (2012).

3 Boyd, A. W. & Lackmann, M. Signals from Eph and ephrin proteins: a developmental tool kit. *Sci STKE* **2001**, re20. (2001).

4 Seiradake, E., Harlos, K., Sutton, G., Aricescu, A. R. & Jones, E. Y. An extracellular steric seeding mechanism for Eph–ephrin signaling platform assembly. *Nat Struct Mol Biol* **17**, 398–402 (2010).

5 Himanen, J. P. *et al.* Architecture of Eph receptor clusters. *Proc Natl Acad Sci U S A* **107**, 10860–10865 (2010).

6 Aricescu, A. R., Lu, W. & Jones, E. Y. A time- and cost-efficient system for high-level protein production in mammalian cells. *Acta Crystallogr D Biol Crystallogr* **62**, 1243–1250 (2006).

7 Grueninger-Leitch, F., D'Arcy, A., D'Arcy, B. & Chene, C. Deglycosylation of proteins for crystallization using recombinant fusion protein glycosidases. *Protein Sci* **5**, 2617–2622 (1996).

8 Walter, T. S. *et al.* Lysine methylation as a routine rescue strategy for protein crystallization. *Structure* **14**, 1617–1622 (2006).